Proceedings of the 16th International Conference on Soil Mechanics and Geotechnical Engineering

doi:10.3233/978-1-61499-656-9-1513

Geotechnical analyses of Taipei International Financial Center (Taipei 101) Construction Project

Analyse géotechnique du projet de construction du Centre International Financier de Taipei (Taipei 101)

D.G. Lin
Department of Soil and Water Conservation National Chung-Hsing University, Taichung, Taiwan 40227
S.M. Woo
Trinity Foundation Engineering Consultants Co., LTD., Taipei, Taiwan

ABSTRACT

This paper presents the results of series of numerical analyses using various simulation schemes to investigate the behavior of piled raft foundation, the possible effect of micro-pile installation on reducing ground movements and the creep deformation of deep excavation in *TIFC* (*T*aipei *I*nternational *F*inancial *C*enter) Construction Project (or Taipei 101 project). The project possesses a large deep excavation area of 152.2*m*×159.14*m*, 5-story basement of 21.7*m* deep and 101-story steel reinforced concrete tower building of 508*m* high. In addition to the pile loading tests in the *TIFC* jobsite which consists of 3 compression piles and 2 extension piles, there totally128 boreholes were drilled for sampling and a series of high quality laboratory tests and field tests were conducted to determine the physical and mechanical properties of soil stratum. Moreover, a well-organized instrumentation system was also established to monitor various ground responses and structural performances during the excavation.

RESUME

Cette thèse présente les résultats des analyses numériques sur la recherche d'une variété des techniques et des manoeuvres possibles pour la construction du « Centre Financement International de Taipei » (Taipei International Financial Center : TIFC) ou appelé « Projet 101 de Taipei. » Cette recherche vise à savoir : 1. Le rôle et la capacité du support des piliers-radeaux dans cette construction. 2. Au cours d'une excavation profonde, l'installation des micro-piliers pourrait-elle possible de réduire le mouvement et la déformation potentiel de la strate. Le projet 101 de Taipei possède une surface de 152.20*m* × 159.14*m* à excaver profondément. Le sous-sol en tout mesure 21.7*m* de profondeur, partagé en 5 niveaux, et la hauteur des 101 étages font 508*m*, l'ensemble est soutenu, renforcé et construit par une structure armée de béton. En outre, sur place, nous avons testé la capacité du chargement des piliers. Le premier consiste à tester 3 groupes des piliers , leurs capacités de résister à la compression. Le second est de savoir leurs capacités de résister à l'extension. Pour ce peojet, en total, il y a 128 endroits ont été creusés pour obtenir les échantillons. Par la suite, avec ceux-ci, nous avons réalisé une série des testes de haute qualité sur le terrain et dans le laboratoire pour déterminer la physique et la mécanique rationnelle de chaque strate. Par ailleurs, au cours de l'excavation et la construction du Centre Financement International de Taipei (101 de Taipei), nous avons systématiquement contrôlé et testé la réaction de la strate et la structure du support.

1 INTRODUCTION

This paper investigated the raft-pile-soil interaction for vertically loaded raft on layered Taipei subsoil by three-dimensional (3-D) numerical analysis. The required input parameters for the analysis were back calculated from the static pile loading tests implemented in the *TIFC* jobsite. There totally 5 static extension and compression pile loading tests were analyzed. Subsequently, the influence of various raft thickness t (1, 2, and 3m), pile spacing s (2d, 3d and 4.5d),where d=pile diameter=2m, pile group configurations (8×8, 5×5, and 3×3) and loading intensity q (1,000, 750, and 400 kPa) on the performance of piled-raft foundation in typical Taipei Subsoil were detected.

To evaluate the effectiveness of micro-pile protection on reducing ground movements during excavation; one row of micro-pile was installed numerically behind the diaphragm wall. An elastic-plastic 3-D numerical analysis incorporated with groundwater flow calculation was performed to calibrate the full-scale deformation behaviors of deep excavation. Eventually, a systematic 3-D analysis was conducted on various installation parameters such as pile inclination (θ), pile spacing ratio (S/D) and pile length (L_m) of micro-pile for a typical deep excavation in Taipei Subsoil.

In addition, a series of axis-symmetric numerical experiment of triaxial lateral unloading creep tests were conducted on Taipei silty clay specimens under various creep stress levels for numerical verification. Two-dimensional numerial analysis of undrained creep analysis with *C*reep *S*oft *S*oil (*C*-*S*-*S*) model was then performed to simulate the creep deformation of deep excavation in *TIFC* construction.

2 CHARATERISTICS OF GROUND MOVEMENTS

As shown in Fig. 1 the measured data points of Taipei 101 project were plotted together with the empirical relationship between maximum ground settlement (S_{vm}) and maximum lateral wall movement (D_{hm}) produced by Mana and Clough (1981) and Ou (1988) from data in varied overall ground conditions in San Francisco and Taipei Basin. The sloid line represents the results of regression calculation. It was indicated that empirical relationship of deep excavation in Taipei 101 project appear most likely to be (S_{vm}/H_e)=0.5~1.0(D_{hm}/H_e). In which, H_e represents the depth of excavation.

3 LOADS TRANSFER OF PILED-RAFT FOUNDATION

For pile loading tests, the numerical results were calibrated by comparing the load-settlement curves at various levels of pile shaft; load transfer curves and *T*-*Z* curve with those from observations. For piled-raft foundation, the responses due to vertical loading were evalueated by load carrying ratio of raft.

3.1 *Geometry and material models*

Figure 2 illustrates the element size at different zones for the analysis of piled raft system. In the analysis, the soil mass was discretized into tetrahedron soil element, the raft foundation and pile structures were modeled by shell element and pile element respectively.

To avoid enormous computation time due to large number of finite difference block element generated by soil~pile system, Taipei Subsoil profile was simplified and simulated by Mohr-Coulomb (*M-C*) model whereas the raft and pile structure by linear elastic (*L-E*) model. The required material model parameters for piled raft system were tabulated in Table 1 and the associated soil~pile interface parameters for pile element were back calculated from the numerical simulations of pile loading test.

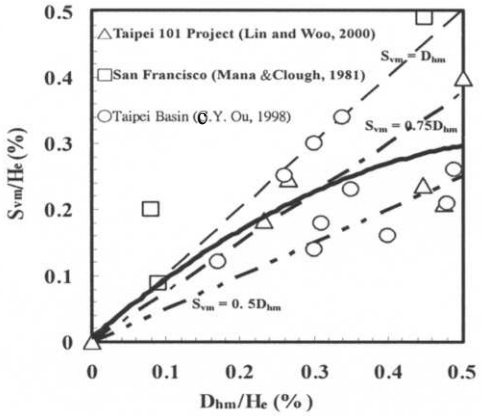

Figure 1. Empirical relationship between maximum ground settlement and maximum lateral movement.

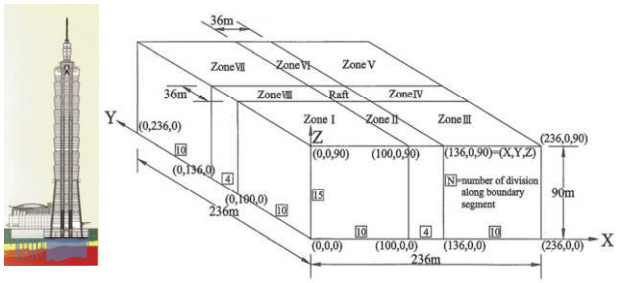

Figure 2. Different zones for element division in piled raft system.

Table 1: Input material model parameters for piled raft system

Depth (*m*) Soil layer	*C* (*kPa*)	ϕ (°)	ν	*E* (*MPa*)	γ_d (kN/m^3)	ψ (°)	f_t (*kPa*)
0~30 Silty clay	20	32	0.3	34.2	16.0	0	32
30~60 Sandstone	100	45	0.3	334.8	19.2	3	100
Raft	Thickness (*m*) 3		0.16	33500	23.5	B_R (*m*)×L_R (*m*) 36×36	
Pile	Diameter (*m*) 2		0.16	33500	23.5	Pile Length (*m*) 50	

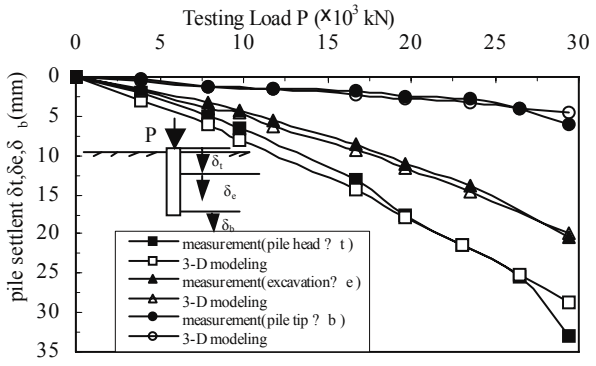

Figure 3. Load-settlement curve of compression loading test at different pile elevation (testing pile *P241*, Lin and Woo, 2000).

3.2 *Load~settlement curves of pile loading test*

For pile loading test (P_d=design load=$1.2\times10^4 kN$), as shown in Fig. 3, a good agreement between numerical predictions and measurements was observed. However, the numerical modeling underestimated the settlement at the final loading increment (underestimation of 10.8% at pile head whereas 25% at pile tip) and the corresponding maximum testing load (P_{max}=29,429*kN*) is approximate to $2.45P_d$. This indicates that the *M-C* soil model is validated for a wide range of loading level.

3.3 *Load carrying ratio and effect of pile configuration*

Figure 4 illustrates the individual percentage of loading carried by piles (Q_{Pi}) and by raft (Q_R). As can be seen, the raft shares 43.8% (=R_R=Q_R/Q) of total vertical load (Q) for loading intensity of 1,000 kN/m^2 whereas it appears to be 30.2%, 10% of total vertical load for loading intensities of 750 and 400 kN/m^2. As a result, the loading carried by raft is proportional to the magnitude of building design load. Meanwhile, the piles near raft center may carry higher percentage of loading than those adjacent to raft edge.

As displayed in Fig. 5, the load carrying ratio of raft, R_R, is influenced by the pile configurations of piled raft system. For a specific pile configuration the R_R value increases with the increase of loading intensity, q, while for a specific loading intensity the pile group with smaller pile spacing (8×8 and s=2*d*) carries more building design load (lower R_R value) than that of larger pile spacing. In addition, the maximum settlement of piled raft and the maximum bending moment increases with the increase of pile spacing.

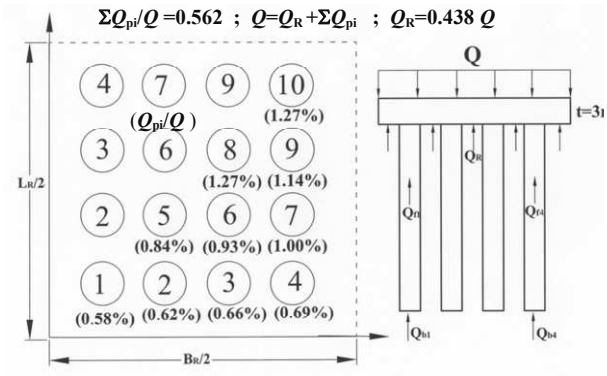

Figure 4. Load carrying ratio of piles at loading of 1000 kN/m^2 (8×8 pile group, *s*=2*d*, *d*=2*m*, B_R×L_R=36*m*×36*m*).

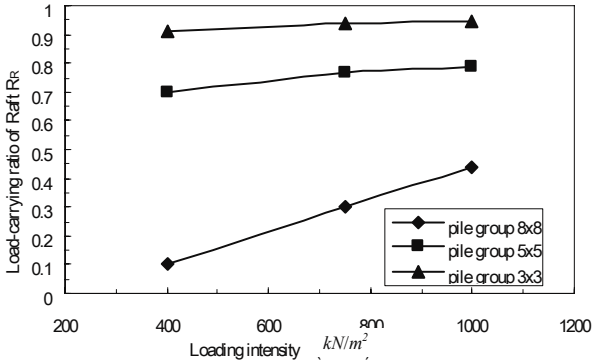

Figure 5. Load-carrying ratio of piled raft of various pile configurations under different loading intensity (raft thickness *t*=3*m*, raft dimension B_R×L_R=36*m*×36*m*).

4 EFFECTS OF MIRO-PILE PROTECTION ON DEEP EXCAVATION

The improvement ratios IR_V (=1-(δ^m_{Vmax} /δ_{Vmax}) and IR_H (=1-(δ^m_{Hmax} /δ_{Hmax})) are defined respectively using the maximum ground settlement (δ_{Vmax} , δ^m_{Vmax}) and the maximum lateral wall movement (δ^m_{Hmax} , δ^m_{Hmax}) with and without micro-pile protection during the excavation. In which, the superscript "*m*" represents the ground movements with micro-pile protection. In the case of deep excavation without micro-pile protection, the IR_V and IR_H values equeal to zero (δ^m_{Vmax} =δ_{Vmax} and δ^m_{Hmax} =δ_{Hmax}).

4.1 *Geometry and material models*

As shown in Fig. 6, the Southeastern corner of deep excavation at Tower Zone was selected for full-scale 3-D analysis and only part of simulation results were presented. In addition, based on the previous research (Lin and Woo, 2000) the typical soil layers for *TIFC* field site can be determined.

Figure 7 illustrates the mesh density at different zones for finite difference discretization. The element sizes adopted in analysis were varied with the zone blocks. In the analysis the diaphragm wall, steel strut and micro-pile structures were modeled by shell element, beam element and pile element respectively. The required input material model parameters for 3-D analyses are preseted in Tables 2 and 3.

4.2 *Lateral wall movement and pore water pressure*

In order to verifiy the validity of 3-D numerical procedures, comparisons were made between the predictions and observations for lateral wall movement and pore water pressure.

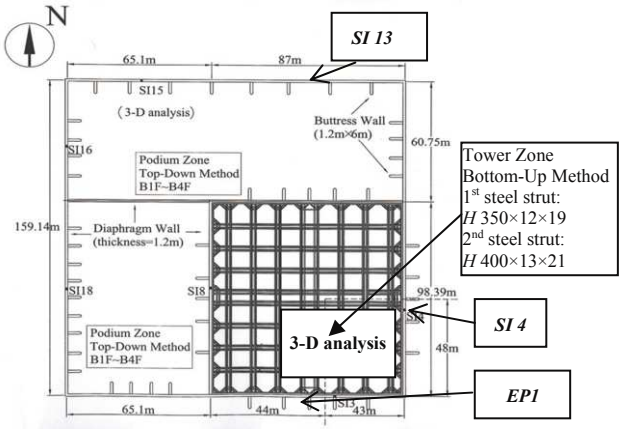

Figure 6. Plan view of excavation layout and selected excavation zone for 3-D analysis.

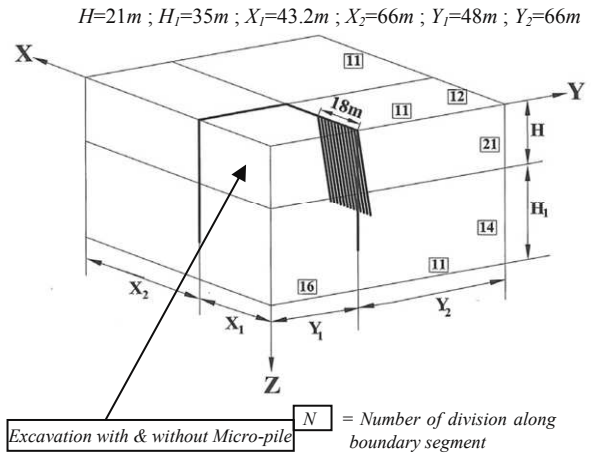

Figure 7. Geometry model for typical excavation in Taipei Metropolitan with and without micro-pile support.

Table 2: Input soil model parameters for full-scale 3-D analysis

Soil Layer	Depth (*m*)	Soil Model	γ_{wet} (γ_d) (kN/m^3) unit weight	*G* ($\times 10^3$) (kPa) shear modulus	*k* ($\times 10^{-7}$) (cm/sec) permeability	ϕ' (^{o})
SF	0~2.2 N=1~12	*M-C*	17.16 (13.00)	1.54		30
CL1a	2.2 ~13.4 N=1~3	*M-C*	17.65 (13.07)	4.25	1.80	25
CL1b	13.4~24.5 N=2~6	*M-C*	17.65 (13.07)	15.0	1.80	26
CL1c	24.5~37.0 N=4~21	*M-C*	17.65 (13.07)	38.17	0.58	30
SM	37.0~42.0 N=9~59	*M-C*	19.12 (15.54)	19.20	2.56	34
CL2	42.0~45.0 N=9~27	*M-C*	18.63 (14.55)	17.40	0.90	30
GC~ GM	45.0~48.0 N=15 or >100	*M-C*	19.41 (15.91)	123.0	517.0	35
SS	48.0~60.0 N>100	*L-E*	2.15 (1.88)	222.0	454.0	39

Table 3: Input material model parameters for structural element

PROPERTY	Shell Element Diaphragm Walls (Concrete Slab)	Beam Element (Steel Strut)
Thickness (*m*) *fc'* =210 (kg/cm^2)	1.2 (0.15 for Floor Slab, 3 for Mat Slab)	H350× 12×19 H400×13×21
Density (kN/m^3)	23.5	77.1
Young's Modulus (*MPa*)	2.13×10^4	2.06×10^5
Poisson's Ratio	0.15	0.30
Steel Struts	4×H350×12×19	4×H400×13×21
Cross-Sectional Area *A* (m^2)	6.956×10^{-2}	8.748×10^{-2}
Second Moment I_x (m^4)	3.756×10^{-3}	6.175×10^{-3}
Second Moment I_y (m^4)	2.844×10^{-3}	4.64×10^{-3}

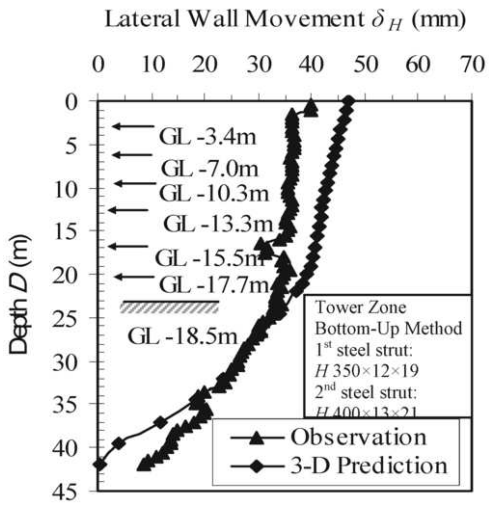

Figure 8. Comparison of lateral wall movement at final excavation stage between 3-D prediction and observation (*SI4*) at Tower Zone.

Figure 8 displays the 3-D prediction of lateral wall movemnt at final excavation stage of inclinometer *SI 4* adjacent to *Sun-Gj Road* and located at a distance of 43*m* from the southeastern corner. The lateral wall movement at different stages of excavation in Tower Zone always appears a cantilever type of movement. As shown in Fig. 9, the variation of pore water pressure at depth of 20*m* and 39.1*m* with elapses time were well predicted.

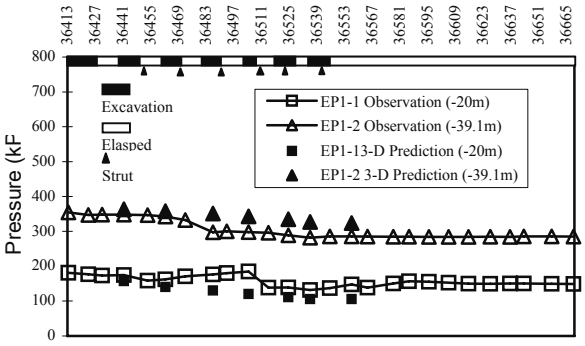

Figure 9. Comparison of pore water pressure between predictions and observations at various excavation stages in Tower Zone.

4.3 *Effects of pile inclination and pile length*

For all cases of pile inclination (θ=5°, 15°, 20° and 30°) and pile length (L_m=20, 30, 35 and 40*m*), the maximum lateral wall movement and ground settlement were reduced with the decrease of spacing/diameter ratio (*S*/*D*).

As shown in Fig. 10, for a specific pile length (L_m=30*m*) except for smaller pile inclinations (θ=5° and 10°), a high improvement ratio of ground settlement IR_V (66~43%) can be achieved. In contrast, for the identical situation only relatively low improvement ratio of lateral wall movement IR_H (6.0~4.0%) were obtained. This implied the effect of micro-pile on reducing lateral wall movement is not as beneficial as on reducing ground settlement. Considering both IR_V and IR_H performances, an optimum pile inclination θ of 15° was proposed for micro-pile construction. Based on numerical results, an optimum pile length of 30*m* is proposed to be efficient in reducing the ground movements for a typical excavation depth of 20*m* (*H*) and a length/depth ratio (=L_m/*H*) of 1.5.

5 CREEP BEHAVIOURS

According to the lateral unloading constant-deviator-stress triaxial undrained creep tests of Taipei silty clay, the deviator stress is applied by lateral unloading to simulate the stress conditions induced by excavation. Specimens with *OCR*=1 were tested by different creep stress levels (*D*s =σ_d/S_u). In which, σ_d and S_u represent the deviator stress applied for creep test and the static undrained shear strength respectively.

5.1 *Lateral unloading triaxial creep testsl*

As presented in Fig. 11, the creep axial strain at the initial unloading stage was underestimated and the predicted tendency appears to agree with that of measurement to a certain extent. In creep simulation, the creep parameter μ^* in *C*-*S*-*S* model is dependent on creep stress level and needs to be adjusted with the creep rate (dε/d*t*).

5.2 *Creep movement of deep excavation*

As shown in Fig. 12, the numerical prediction of creep deformation of inclinometer *SI13* (at *N*-*S* cross-section) at Podium Zone were performed for a period of time (2000, 01/22~2000, 04/04) Subsequently, a creep rate of 0.34 *mm*/*day* for 24 days creep time duration was observed at the wall depth of 13*m* after completing 3rd stage excavation (excavation depth of 13.15*m*).

6 CONCLUSIONS

According to the numerical results, the piled raft is capable of sharing 43.8% of the total vertical load as the loading intensity reaches 1,000 *kPa*. The effect of micro-pile on reducing lateral wall movement is not as beneficial as on reducing ground settlement.

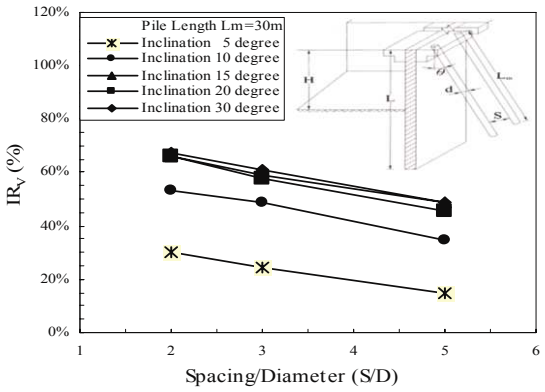

Figure 10. Effect of micro-pile inclination on improvement ratio of ground settlement.

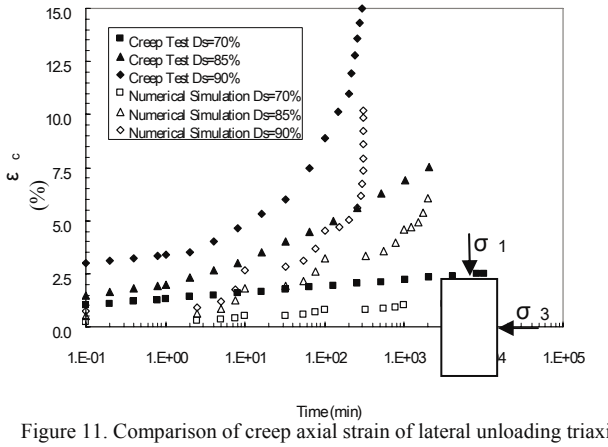

Figure 11. Comparison of creep axial strain of lateral unloading triaxia creep test at various deviator stress levels (*D*s).

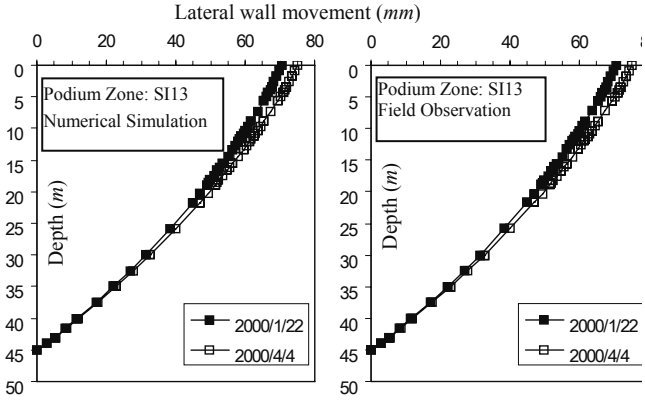

Figure 12. Lateral wall creep movement in Podium Zone (4.4*m* excavatio depth) after the excavation of Tower Zone (21.7*m* excavation depth).

REFERENCES

Lin D.G. and Woo S.M. 2000. Deformation analysis of Taipei International Financial Center deep excavation project, *Technical Report. Trinity Foundation Engineering Consultants Co., LTD*.

Mana A.I. and Clough G.W. 1981. Prediction of movements for braced cuts in clay. *J. Geotech. Engng, ASCE*, 1981, 107, June, 759-777.

Ou, C.Y., J.T. Liao, and H.D. Lin 1998. Performance of diaphragm wall constructed using top-down method. *J. of Geotech. and Geoenvironmental Engn., ASCE*, Vol. 124, No. 9, pp. 987-808.